High-Resolution Mapping of Postinfarction Reentrant Ventricular Tachycardia

Electrophysiological Characterization of the Circuit

Elad Anter, MD
Cory M. Tschabrunn, CEPS
Alfred E. Buxton, MD
Mark E. Josephson, MD

BACKGROUND: In vivo description of ventricular tachycardia (VT) circuits is limited by insufficient spatiotemporal resolution. We used a novel high-resolution mapping technology to characterize the electrophysiological properties of the postinfarction reentrant VT circuit.

METHODS: In 15 swine, myocardial infarction was induced by left anterior descending artery balloon occlusion. Animals were studied 6 to 8 weeks after myocardial infarction. Activation mapping of VTs was performed by using the Rhythmia mapping system. Activation time was based on a combination of bipolar and unipolar electrograms. The response to overdrive pacing from different zones of the circuit was examined.

RESULTS: A total of 56 monomorphic VTs were induced (3.8±2.1 per animal). Among these, 21 (37.5%) were hemodynamically stable and allowed mapping of the circuit. Isthmuses were 16.4±7.2 mm long and 7.4±2.8 mm wide. Conduction velocities were slowest at the inward curvature into the isthmus entrance (0.28±0.2 m/s), slightly faster at the outward curvature exit (0.40±0.3 m/s) and nearly normal at the central isthmus (0.62±0.2 m/s). In 3 animals, 2 VT morphologies with opposite axes sharing the same isthmus were mapped. Conduction velocities within the shared isthmus were dependent on the activation vector, consistently slower at the proximal curvature. Overdrive pacing from isthmus sites determined by activation mapping was consistent with entrainment criteria for isthmus. However, dimensions of the isthmus defined by entrainment exceeded dimensions of the isthmus measured by activation mapping by 32±18%.

CONCLUSIONS: In postinfarction reentrant VT, conduction velocities are slowest at the proximal and distal curvatures. Entrainment mapping overestimates the true size of the isthmus. High-resolution activation mapping of VT may better guide ablation therapy.

Correspondence to: Elad Anter, MD, Harvard-Thorndike Electrophysiology Institute, Beth Israel Deaconess Medical Center, 185 Pilgrim Rd, Baker 4, Boston, MA 02215. E-mail eanter@bidmc.harvard.edu

Sources of Funding, see page 326

Key Words: cardiac ablation ■ electrophysiology ■ intracardiac electrograms ■ mapping ■ myocardial infarction ■ ventricular tachycardia

Circulation. 2016;134:314–327. DOI: 10.1161/CIRCULATIONAHA.116.021955

CLINICAL PERSPECTIVE

What Is New?

- The common channel isthmus of infarct-related ventricular tachycardia circuits is formed by functional rather than fixed line(s) of block: the lateral boundaries of the isthmus allow conduction through them that is sufficiently slow to protect the common channel and allow propagation of the orthodromic wave front.
- The zone(s) of slow conduction within the reentrant circuit are the inward (entrance) and outward (exit) curvatures, while conduction velocity in the common channel itself is nearly normal.
- Entrainment mapping overestimates dimensions of the isthmus. Specifically, exit sites based on entrainment criteria may be well past the true exit as determined by activation.

What Are the Clinical Implications?

- Barriers forming the isthmus during ventricular tachycardia are not always present during sinus rhythm, highlighting the limitations of current substrate-based mapping techniques.
- Because conduction slowing is a prerequisite for reentry to occur, ablation at zones of high curvature may be an attractive target for ablation.
- Entrainment from true exit sites within or proximal to the outward curvature have postpacing interval values of ≤10 ms.

Sustained monomorphic ventricular tachycardia (VT) attributable to previous myocardial infarction is usually caused by myocardial reentry in the so-called border zone of the infarct.[1–3] In this zone, coupling between muscle bundles is reduced because of fibrosis, diminished gap junction density, and alternation in gap junction distribution and function.[4,5] This can result in either fixed or functional conduction block facilitating reentry using a protected channel isthmus.[6]

Mapping reentrant VTs is a clinical challenge and difficult to achieve. Activation and entrainment mapping can localize the circuit including its protected isthmus; however, this is often time consuming and limited to hemodynamically tolerated arrhythmias. As a result, ablation strategies are often limited to substrate mapping (low voltage and abnormal electrograms). Although this approach can be effective in postinfarction patients, arrhythmia recurrence is common.[7] One limitation of substrate-based mapping stems from the fact that lines of block including the protected isthmus may be partially functional with relative paucity of abnormal electrograms during sinus rhythm.[8] As such, activation mapping of VT remains a desired strategy. It can identify isthmuses formed by either fixed or functional lines of conduction block. Termination with ablation is a proof that the targeted tissue is clinically relevant. Last, it may theoretically require less ablation.

There has been increasing interest to develop technologies that allow detailed and rapid activation mapping of arrhythmias. This includes catheters with multiple small and closely spaced electrodes, accurate time annotation of multicomponent electrograms, and software allowing automated rapid data collection. In this study, we used the Rhythmia high-resolution mapping system to: (1) examine the feasibility of mapping postinfarction reentrant VTs, (2) examine the electrophysiological properties of the isthmus, and (3) correlate the relationship between isthmus determined by activation and entrainment mapping.

METHODS

Swine Infarct Model

We studied 15 swine with chronic anterior wall infarction. Our swine model has been recently described and closely approximates human subendocardial infarction and reentrant VT.[9] In brief, Yorkshire swine (male, 30–35 kg) underwent selective balloon occlusion of the left anterior descending artery for duration of 180 minutes. After 6 to 8 weeks, the animals underwent an electrophysiology study and mapping of VT. Cardiac MRI was performed 1 to 3 days before the electrophysiology study. This research was performed at the Beth Israel Deaconess Medical Center, Experimental Electrophysiology Laboratory in Boston, MA. The institutional animal care and use committee approved this research protocol.

Electrophysiology Study

The electrophysiology study was performed under general anesthesia with isoflurane inhalation. Percutaneous femoral arterial and venous access were obtained. Under fluoroscopic guidance, a 6F pentapolar diagnostic catheter (Bard EP, Lowell, MA) was placed in the right ventricular (RV) apex to allow pacing and to act as an intracardiac activation reference. The proximal electrode was positioned in the inferior vena cava and served as an indifferent unipolar electrode. Unfractionated heparin was administered to maintain an activated clotting time of 300 to 400 s for the duration of the procedure.

Electric stimulation was performed from the RV apex using a current strength twice the capture threshold and pulse width of 2.0 ms. Programmed ventricular stimulation at paced cycle lengths of 600 and 400 ms with 1 to 4 extrastimuli down to ventricular effective refractory period were performed to induce VT. If electric stimulation from the RV apex failed to induce VT, stimulation was repeated from the RV outflow tract followed by the left ventricle (LV). We attempted to map all hemodynamically tolerated monomorphic VTs. These were defined as VTs with a systolic blood pressure ≥80 mm Hg. If the VT was not hemodynamically tolerated, it was terminated by pacing or electric cardioversion. In these cases, inotropic support (phenylephrine bolus of 5–10 mg) was administered to increase the blood pressure before the next attempt to induce VT. Furthermore, if the tachycardia cycle length (TCL) was ≤220 ms, procainamide (5 mg/kg bolus followed by infusion at a rate of 2–4 mg/min) was administered in an attempt to increase the TCL.

Activation Mapping

Activation mapping was performed using the Rhythmia mapping system with its proprietary Orion 64-electrode minibasket catheter (Boston Scientific, Cambridge, MA). The minibasket catheter is an 8F catheter that consists of 8 splines, each containing 8 small electrodes. The surface area of each electrode is 0.4 mm^2 and the interelectrode spacing is 2.5 mm measured from center to center. The minibasket is expendable to a nominal diameter of 18 mm and a maximal diameter of 22 mm (measured at its equator). The length of the basket from pole to pole is 23 mm.[10] Local activation was determined based on the combination of the bipolar and unipolar electrograms and timed at the maximal (–)dV/dt of the local unipolar electrogram. At sites with multicomponent and fractionated bipolar potentials, the activation time was determined by the maximal (–)dV/dt of the corresponding unipolar electrograms (Figure 1).

Data acquisition during VT was automatic with the following beat acceptance criteria: (1) 12-lead ECG morphology match; (2) TCL stability (±5 ms); (3) time stability of a reference electrogram positioned at the RV apex; (4) beat-to-beat ECG consistency (≥3 beats with similar electrogram morphology and timing); and (5) respiratory stability allowing data acquisition at a constant respiratory phase. Bipolar electrograms were filtered at 30 and 300 Hz. Unipolar electrograms were filtered at 1 and 300 Hz. Selected electrograms had bipolar voltage amplitude >0.03 mV (2-fold higher than the noise level in our laboratory). All electrograms were reviewed offline using electronic calipers at similar gain and paper speed of 200 mm/s.

Mapping of the LV was performed using a retrograde transaortic approach by slowly navigating the steerable minibasket catheter throughout the entire chamber. We attempted to include only data points in contact with the endocardial

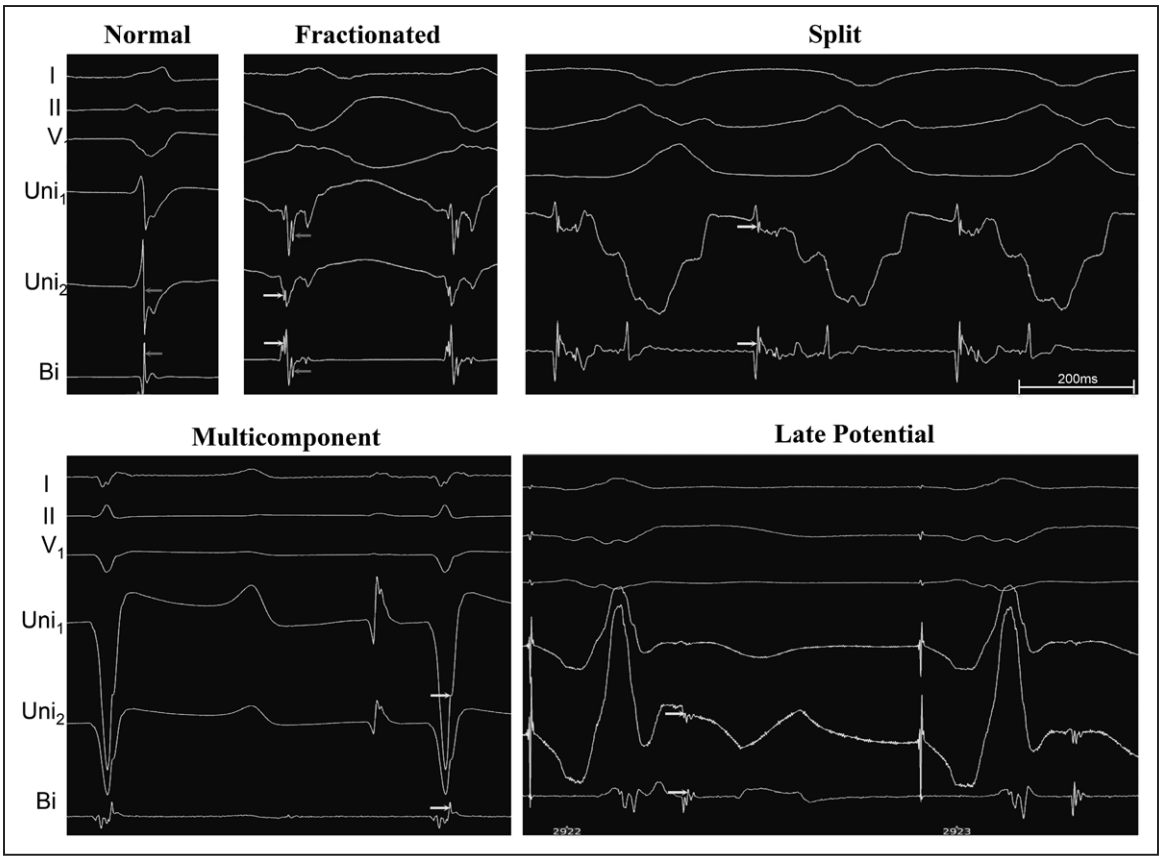

Figure 1. Local time annotation of complex electrograms.
This figure demonstrates the method of local time (activation time) annotation using a combination of bipolar and unipolar electrograms. **Left upper**, Activation time annotation of a normal triphasic electrogram during sinus rhythm. Activation time is annotated at the dV/dt_{max} of the unipolar electrogram (Uni), coinciding with the peak of the bipolar (Bi) electrogram (red arrows). **Middle upper**, Activation time annotation of a fractionated electrogram during ventricular tachycardia (VT). The bipolar electrogram contains 2 separate high-frequency components marked with yellow and red arrows. The first component of the bipolar electrogram coincides with dV/dt_{max} of Uni_2 (yellow arrows), whereas the second component of the bipolar electrogram coincides with dV/dt_{max} of Uni_1 (red arrow). Thus, activation time of this bipolar electrogram is separated into 2: the first component is annotated at the location of Uni_2 and the second component is annotated at the location of Uni_1. **Right upper**, Local activation time of a split electrogram during VT. The local activation time coincides with the peak of the first component (yellow arrow) as determined by the dV/dt_{max} of the unipolar signal. **Left lower**, Activation time annotation of a multicomponent electrogram during sinus rhythm. The local activation time is marked at the terminal component of the bipolar electrogram, coinciding with the dV/dt_{max} of the unipolar signal (yellow arrow). **Right lower**, Activation time annotation of a complex split and multicomponent electrogram during right ventricular paced rhythm. The local activation time is marked at the late potential based on the maximal dV/dt.

surface. This included points within 2 mm from the cardiac MRI registered LV endocardial surface that had ≥3 consecutive beats with similar and distinct near-field electrogram morphology and stable activation timing.

Following completion of the activation map, the unipolar data were displayed using isochrones drawn at 10-ms intervals and colored on a color scale from red to purple, intersecting the middiastolic electric phase. Every color band represents conduction over a 10-ms interval.

Definitions Used for Interpretation of Activation Maps

Mapping of a macroreentrant VT was considered complete when: (1) ≥90% of the TCL was mapped; (2) a channel of conduction isthmus was identified; and (3) mapping density at zones of slow conduction was adequate, limiting data interpolation between points to ≤3 mm. The mechanism of the tachycardia was defined as macroreentry or focal on the basis of the activation map. Macroreentrant circuits had a well-defined entrance site (inward curvature), common pathway (isthmus), and separate exit site (outward curvature). The entrance was defined as the site at which the orthodromic wave front enters to the common pathway (inward curvature), whereas the exit was defined as the site at which the orthodromic wave front exits the common pathway (outward curvature). Microreentry was defined as a tachycardia with a point source and centrifugal spread of activation that can be entrained with overdrive pacing. Fractionated signals were defined as those with ≥5 deflections crossing the isoelectric baseline. Split potentials were defined as those with ≥2 separate deflections separated by an isoelectric interval ≥30 ms. Split potentials could have occurred during the QRS or after the QRS (ie, late potentials).

Definition Used for Interpretation of Entrainment Map

After completion of the activation map, overdrive pacing was performed at selected sites of macroreentrant circuits as determined by activation mapping. These sites included some or all of the following: (1) inward curvature entrance, (2) isthmus common channel, (3) outward curvature exit, and (4) remote RV and LV sites. The number of pacing sites during VT depended on the hemodynamic tolerance of the arrhythmia. Pacing was performed from the minibasket electrodes at a cycle length 10 to 25 ms faster than the TCL. If pacing entrained the tachycardia with concealed fusion, the postpacing interval (PPI) and the S-QRS were analyzed to determine whether the site was in the reentry circuit using conventional criteria.[11] Concealed fusion was considered when the pacing morphology was identical to the VT morphology at all 12 ECG leads. The PPI was measured from the pacing stimulus of the last paced beat to the initial deflection of the first return VT beat at the pacing site. A pacing site demonstrating concealed fusion, PPI-TCL ≤30ms, and S-QRS ≤70% TCL was considered to be located within a protected isthmus of the reentrant circuit.

Measurement of Isthmus Dimensions

Dimensions of the isthmus (common channel) were calculated separately from the activation and entrainment maps. From the activation map, the length of the isthmus was measured as the shortest distance between the proximal curvature entrance to the distal curvature exit of the common channel, whereas its width was measured from one apparently nonconductive lateral barrier to the opposing parallel nonconductive barrier. Dimensions of the common channel using entrainment were based on the zone that includes sites with concealed QRS fusion, PPI-TCL ≤30 ms, and S-QRS of 0% to 70% of the TCL.

Measurement of Propagation Velocity

Assessment of conduction velocity in the reentrant circuit was calculated by using the single-vector method from the high-density endocardial mapping defined as ≥25 points/cm^2.[12,13] In brief, recording sites were selected on a line longitudinal and perpendicular to the isochronal lines. The longitudinal and transverse conduction velocities were calculated from the difference in timing and the known distance between the recording points. Conduction velocity was then calculated for the mean vector of propagation.

Statistical Analysis

Descriptive statistics are reported as mean±standard deviation, median, and range for continuous variables and as absolute frequencies and percentages for categorical variables. Comparison between conduction velocities at different zones of the reentrant circuit for each VT was calculated using the ratio paired Student *t* test and reported as the logarithmic value of the ratio with the 95% confidence interval. Comparison between differences of mean velocity in each zone of the circuit for all VTs was calculated by using the unpaired Student *t* test. Comparison between dimensions of the isthmus as measured by activation and entrainment mapping was performed using the paired Student *t* test. A *P* value of <0.05 was considered statistically significant. Analyses were conducted using Prism 6 (La Jolla, CA).

RESULTS

VT Characteristics

A total of 56 sustained monomorphic VTs were induced in 15 swine (3.8±2.1; median 3; 1–5). Among these, 21 VTs (37.5%) were hemodynamically tolerated and sustained for 7.2±3.7 minutes (median 8; 5–12). Activation mapping of these VTs was consistent with a macroreentry mechanism in 18 of 21 tachycardias (86%) and focal origin in 3 of 21 tachycardias (14%). The mean TCL of the mapped VTs was 324±124 ms (median 346; 260–435). The predominant axes were left-bundle left superior (43%), right-bundle left superior (29%), and left-bundle right inferior axis (14%). Cardiac MRI demonstrated late gadolinium enhancement in the anterior septum with wall motion abnormalities and an overall reduced LV ejection fraction of 37.5±12.

Activation Mapping of the Macroreentrant Circuit

Mapping Resolution

The mean number of activation points per VT map was 8240±3326 (median 9080; 4916–21 118). The mean number of activation points per square centimeter of

endocardial surface area was 82±66 (median 52; 16–148). This dense activation map permitted constructing detailed activation maps. Figure 2 shows activation maps of 2 mapped VTs. Movie I in the online-only Data Supplement shows the propagation map of a reentrant VT. The most frequent circuit shape was figure-eight reentry circuit (14/18) followed by a single-loop reentry circuit (2/18), and Y-shaped reentry circuit (2/18; Figures 2 and 3).

The 64-electrode basket catheter acquired an average of 12±6 (median 12; 4–18) electrograms at each tachycardia beat. This is because the circular basket catheter only had an average of 2 splines that were in contact with the endocardial wall, whereas the remaining 6 splines were facing the blood pool.

Characteristics of the Common Channel

Proximal Curvature (Entrance)

At entrance sites, the linear excitation wave front assumed a curved shape. The excitation wave front curved inward (convex) and propagated slowly toward the common channel (Movie I in the online-only Data Supplement). At this proximal curvature, conduction velocities become slower in comparison with the outer loop by a factor of 0.52 (95% confidence interval, 0.45–0.58; $P<0.001$). The mean conduction velocity decreased from 0.78±0.2 to 0.28±0.2 m/s ($P<0.01$). Figure 3 shows isochronal map of propagation derived from the dV/dt_{max} within the reentrant circuit. Conduction velocities at the proximal curvature were the slowest in the reentrant circuit as shown by increased isochronal density, occupying 32% (median 36%; 24%–45%) of the TCL.

At this curved zone of slow conduction, electrograms during VT were predominantly fractionated (85%; 1780/2100). Split potentials were also present (24%; 496/2100). Figure 4 shows frequent electrograms present at each zone of the reentrant circuit.

Common Channel (Midisthmus)

The common channel was characterized by linear propagation in a 2-dimensional structure bounded by 2 laterally opposing zones of very slow conduction propagating in a transverse orientation to the orthodromic wave front (Figure 3). As the excitation wave front entered the common channel, conduction velocities became faster in comparison with the proximal curvature by a factor of 2.88 (95% confidence interval, 1.89–4.16; $P<0.01$). The mean conduction velocity increased from 0.28±0.2 to 0.62±0.2 m/s ($P<0.01$). The more rapid conduction velocity at the common channel is demonstrated by reduced isochronal density. The parallel lateral boundaries of the common channel were similar in length in 7 of 18 (39%) and different in lengths in 11 of 18 (61%) as demonstrated in Figure 4, highlighting the complex structure of the isthmus.

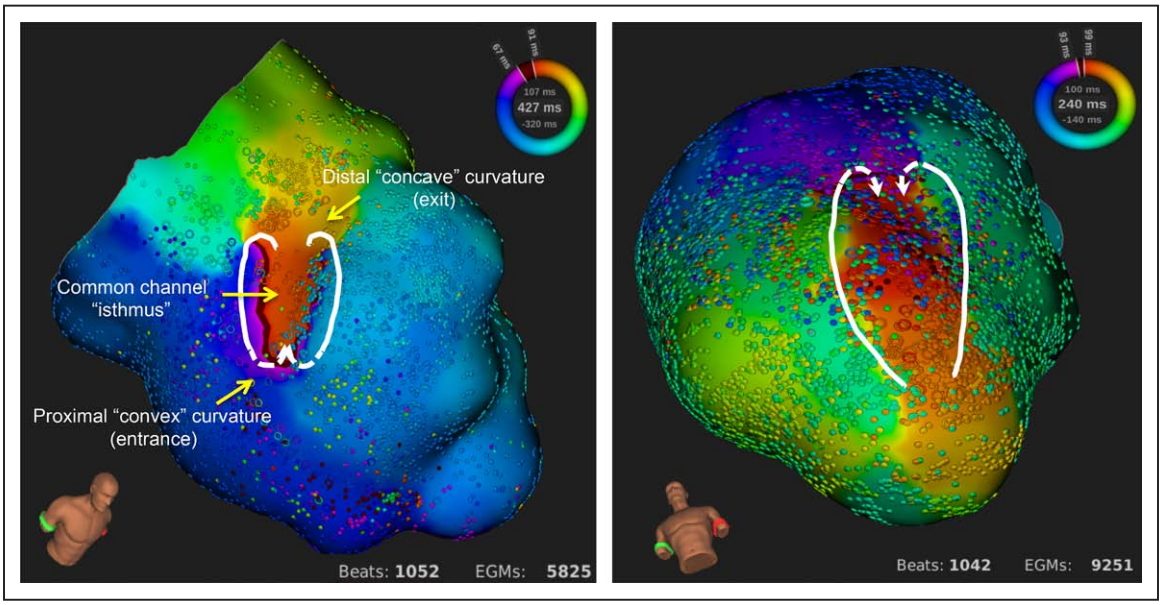

Figure 2. Activation map of reentrant ventricular tachycardias.
Activation maps of ventricular tachycardias (VT) in the anterior-septum of the left ventricle. **Left**, Reentrant figure-eight circuit with a separate entrance, common channel, and exit. The entrance is characterized by convergence of the 2 activation wave fronts, forming a convex-shaped curvature with a wave front propagating toward the common channel. The common channel isthmus is bounded by 2 lateral lines of block (or pseudoblock, allowing very slow conduction). The exit is characterized by concave-shaped curvature with divergence of wave fronts in front and lateral to the common channel. **Right**, Another example of figure-eight reentrant VT with an opposite axis. The arrowheads mark the proximal curvature (entrance) into the common channel. EGM indicates electrogram.

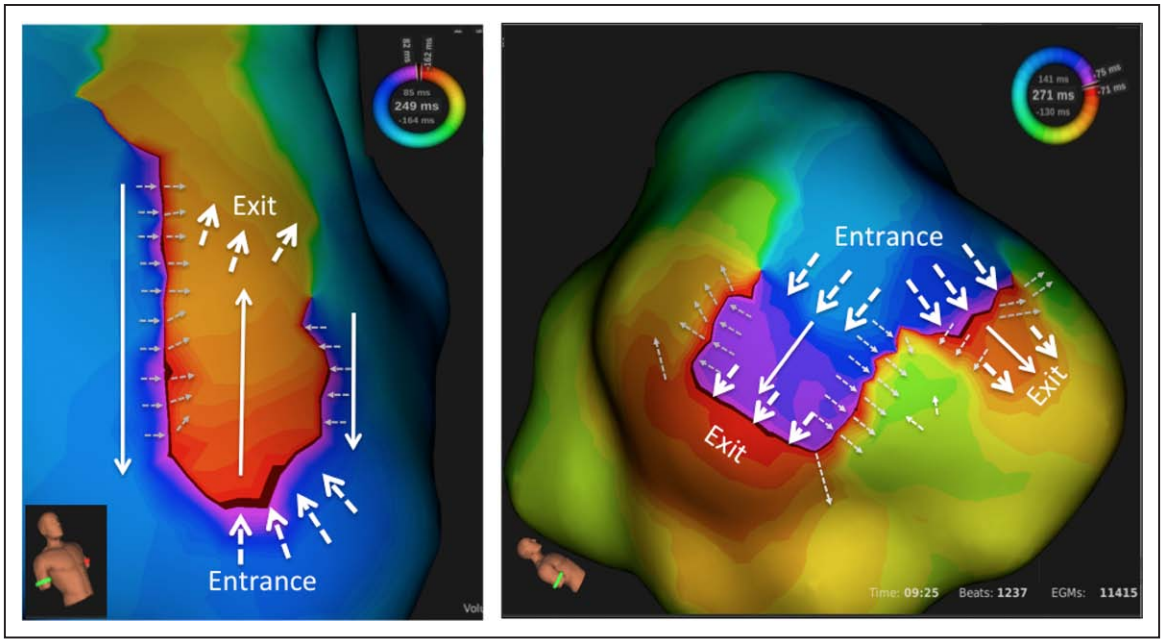

Figure 3. Isochronal maps of reentrant ventricular tachycardia.
Isochronal maps (10-ms steps) derived from the unipolar dV/dt_{max} of the 2 ventricular tachycardia (VT) circuits. **Left**, Figure-eight reentrant VT with increased isochronal density at the proximal curvature (entrance), suggestive of decreased conduction velocity (dashed white arrows). Conduction velocity within the common channel is increased as suggested by reduced isochronal density (solid white arrow). At the distal curvature (exit), conduction velocity is again slowed as demonstrated by increased isochronal density (dashed white arrows). The lateral boundaries of the isthmus are characterized by increased isochronal density suggestive of conduction of slowing (gray dashed arrows). Conduction along the outer boundaries of the isthmus, in the outer loop, is rapid and opposite in direction to the orthodromic wave front of the common channel (white arrows). **Right**, Isochronal map of a Y-shaped reentrant VT circuit with similar conduction velocity pattern. Conduction velocities are slowest at the proximal and distal curvatures but nearly normal in the common channel.

The lateral boundaries of the isthmus did not form lines of complete conduction block, but rather allowed slow transverse conduction through them, consistent with pseudoblock rather than the true line of conduction block (Figure 3). The transverse conduction velocity across the lateral boundaries was 0.05±0.02 m/s, sufficiently slow to protect the common channel and allow propagation of the orthodromic wave front.

Electrograms at the common channel were predominantly split (90%; 3790/4223) whereas fractionated signals were less common (41%; 1739/4223). Split potentials frequently showed opposite unipolar electrogram polarity with an 180° difference in the activation vector, consistent with 1 wave front propagating orthodromically in the isthmus and a second wave front propagating in the opposite direction at the outer loop (Figure 4).

Distal Curvature (Exit)

The distal curvature exit was characterized by outward (concave) curvature of the activation wave front with significant conduction velocity slowing in comparison with the common channel. At exit sites, conduction velocities become slower than the common channel by a factor of 0.66 (95% confidence interval, 0.38–0.72; P=0.022). The mean conduction velocity slowed from 0.62±0.2 to 0.40±0.3 m/s (P<0.01). At exit sites, linear wave front propagation assumed a curved shape. The excitation front curved outward (concave) and propagated slowly as showed by increased isochronal density (Figure 3).

At this curved zone, electrograms were predominantly fractionated (87%; 4501/5174). Split potentials were also present frequent (39%; 2024/5174). Figure 4 shows typical electrograms present at exit sites.

Outer Loop

The outer loop was characterized by linear propagation of the excitation wave front along the outer borders of the common channel (Figure 3 and Movie I in the online-only Data Supplement). The vector of propagation in the outer loop was 180° opposite to the orthodromic wave front of the common channel. Electrograms at the outer loop were predominantly split (78%; 3298/4227) similar to electrograms recorded in the common channel (Figure 4). However, in contrast to electrograms recorded in the common channel, the local outer loop signal occurred during ventricular activation within the QRS complex, whereas the second signal originating in the common channel occurred during electric diastole.

In 3 animals, 2 distinct VT morphologies with opposite axes were mapped (total of 6 VTs). In these cases,

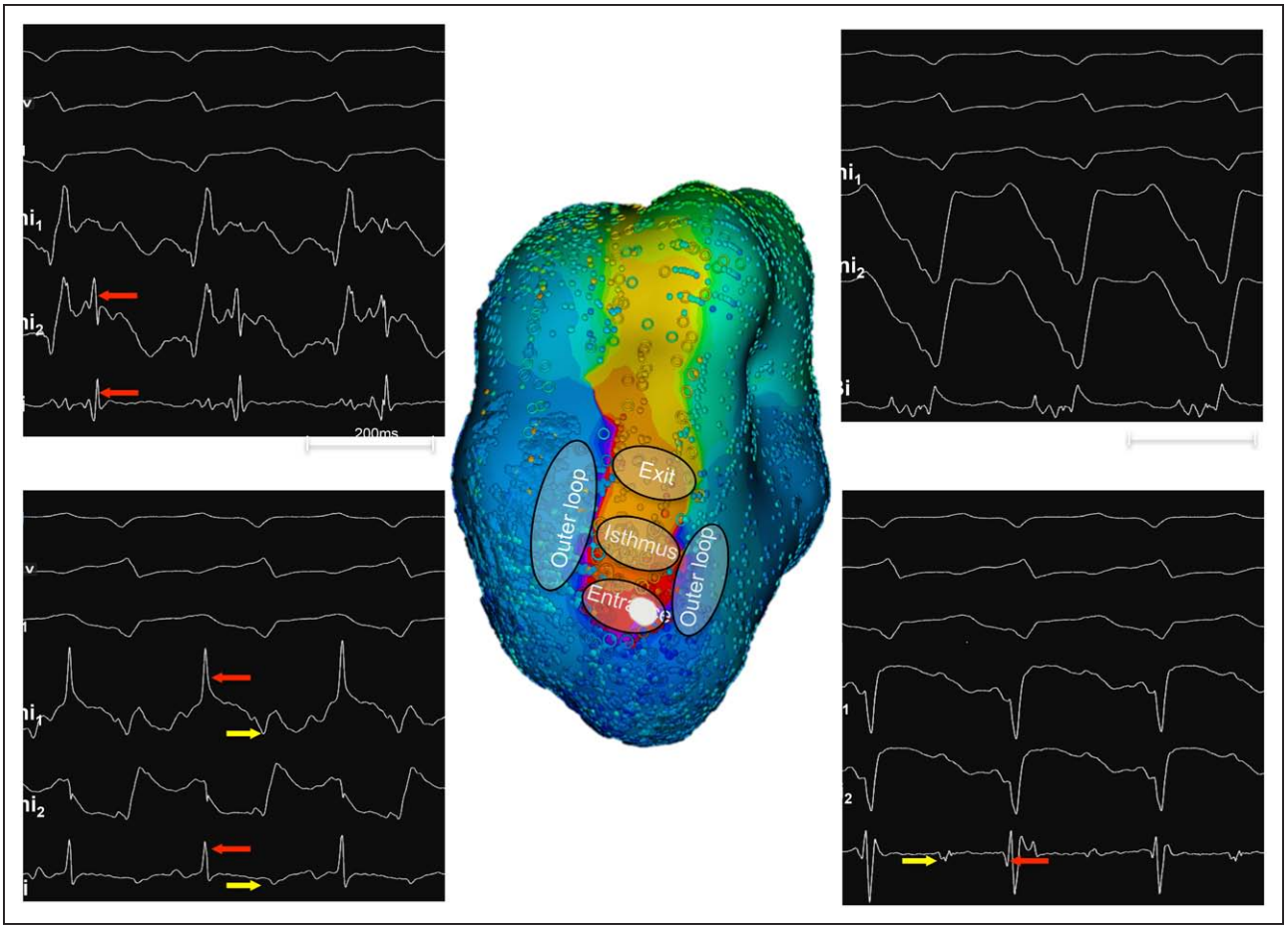

Figure 4. Electrogram characteristics at various zones of the reentrant circuit.
This figure shows 4 panels with electrogram characteristics of entrance, isthmus, exit, and outer loop of a reentrant ventricular tachycardia circuit. Each panel includes 3 surface electrocardiographic leads (I, II, V_1), bipolar (Bi) electrogram with its 2 corresponding unipolar (Uni_1 and Uni_2) electrograms. **Left upper**, Characteristic electrogram recorded at an entrance site. The bipolar electrogram is fractionated and of long duration. This is attributable to increased curvature with slower conduction velocity at the entrance zone. The local activation time is at the early diastole (red arrow) as determined by the dV/dt_{max} of the unipolar electrogram. **Left lower**, Characteristic electrogram recorded at an isthmus site. The bipolar electrogram displays a split signal with a near-field middiastolic signal (red arrow) and a far-field systolic signal (yellow arrow). The diastolic signal derives from the orthodromic wave front propagation within the common channel, whereas the systolic signal derives from the wave front propagating in the opposite direction at the outer loop. This is demonstrated by the reverse electrogram polarity of the unipolar electrogram. **Right upper**, Characteristic electrogram recorded at an exit site, displaying a fractionated signal, consistent with increased curvature with slower conduction velocity at exit sites. **Right lower**, Characteristic electrogram recorded at outer loop sites. The bipolar electrogram is split similar to electrograms recorded at isthmus sites. However, in contrast to electrograms recorded in the isthmus, the local near-field signal determined by the unipolar dV/dt_{max} occurs during ventricular activation (red arrow), whereas the far-field signal originating in the isthmus occurs during diastole (yellow arrow).

entrance of one VT became the exit of the second VT. These cases allowed us to examine whether conduction velocities in the circuit were fixed or rather influenced by the wave front vector of the tachycardia. Conduction velocities were consistently slower at the zones of curvature than at the noncurved zone of linear wave front propagation. Furthermore, conduction velocities were slowest at the inward curvature, such that when the exit of 1 VT became the entrance of a second VT, conduction velocities at the entrance site decreased from 0.44±0.2 to 0.29±0.2 m/s; P=0.01 (Figure 5). These data suggest that conduction velocities in the reentrant circuit are not fixed but rather dependent of wave front propagation, and slowest at the inward curvature.

Axis and Dimensions of the Isthmus

A total of 15 distinct isthmuses were identified in 18 macroreentrant VTs mapped. Three VTs shared a common isthmus as described above. The axis of the isthmus was uniformly oriented parallel to the long axis of the ventricle (±30°). As the submyocardial fiber orientation in

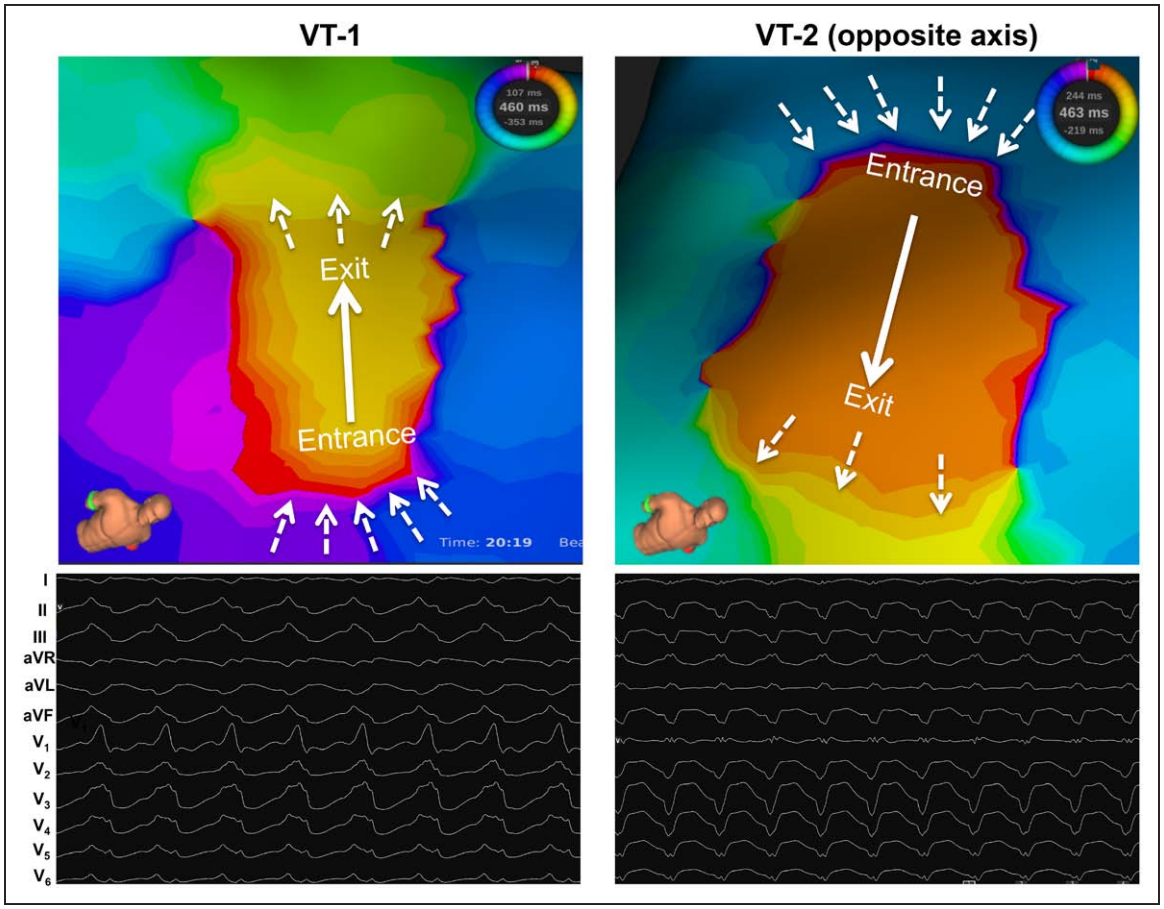

Figure 5. Conduction velocities in the isthmus are influenced by the vector of propagation.
Example of 2 ventricular tachycardias (VTs) with opposite axes sharing 1 isthmus. VT-1 had a right bundle-branch block pattern with an inferior axis, whereas VT-2 had a right bundle-branch block pattern with a superior axis. The tachycardia cycle length was similar at 460 and 463 ms, respectively (**Left** and **Right lower**). The isochronal map of VT-1 shows maximal isochronal density, suggestive of slowest conduction velocity, at the proximal curvature (entrance). Once the wave front reaches the common channel isthmus, conduction velocity is increased as marked by lower isochronal density (solid arrow). At the distal curvature (exit), conduction velocity is slowed again as suggested by increased isochronal density (dashed arrows). During VT-2, the wave front of propagation is reversed, such that the entrance of VT-1 becomes the exit of VT-2 and the exit of VT-1 becomes the entrance of VT-2. The isochronal map of VT-2 shows maximal isochronal density at the proximal curvature (entrance), suggesting that conduction velocity within the circuit is not fixed to the underlying substrate but rather functional, consistently slower at the proximal curvature.

the LV is parallel to the long axis of the ventricle, the axis of the isthmus was also parallel to the submyocardial fiber orientation. The length of the isthmus was 16.4±7.2 mm long (median, 16.2 mm; range, 11.6–23.4 mm). The width of the isthmus was 7.4±2.8 mm (median, 7.8 mm; range, 5.6–16.1 mm).

Entrainment Mapping of the Macroreentrant Circuit

Entrainment From Within the Circuit

Entrainment was performed from 7 proximal isthmus sites (inward curvature entrance), 14 midisthmus sites, 17 distal isthmus sites (outward curvature exit) sites, and 11 outer loop sites. Entrainment from midisthmus sites resulted in concealed QRS fusion and PPI-TCL of 5±2 ms (median 3; 0–8). Entrainment from entrance sites resulted in either concealed QRS fusion (5 VTs) or manifest QRS fusion (2 VTs). In the cases of manifest QRS fusion, the early stimulus at entrance sites propagated antidromically to change the QRS morphology. The PPI-TCL at entrance sites was 16±12 ms (median 8; 0–28). Entrainment from exit sites resulted in concealed QRS fusion and PPI-TCL of 5±5 ms (median 2; 0–10). Entrainment from outer loop sites resulted in QRS fusion and PPI-TCL 9±6 ms (median 5; 0–15).

Entrainment From Outside the Circuit

Entrainment was performed from 34 remote LV and RV sites. Entrainment from these sites resulted in manifest QRS fusion and PPI-TCL of 56±24 ms (median 54; 32–80) in all 8 RV pacing sites and in 12 LV pacing

sites. In 14 LV pacing sites distal to the exit site (median 12 mm; 10–28 mm), entrainment resulted in concealed QRS fusion with PPI-TCL of 22±8 ms (median 20; 14–30). These sites, although outside the circuit as determined by activation mapping, were considered to be within the reentrant circuit as determined by entrainment criteria. These sites were termed pseudoexit sites (Figure 6). In comparison to true exit sites, pseudoexit sites had longer PPI and shorter S-QRS. The Table summarizes the electrogram characteristics and response to entrainment in various parts of the reentrant circuit.

Dimensions of the Isthmus: Comparison Between Activation and Entrainment Mapping

In 11 VTs, detailed interrogation of the isthmus with entrainment mapping allowed measurement of its length. The length of the isthmus measured by entrainment mapping was 22% to 50% longer than the same isthmus defined by activation mapping (23.4±8.0 mm[12.8–36.0 mm] versus 18.4±7.2 mm [11.6–23.4 mm]; *P*=0.04). The increased length of the isthmus measured with entrainment was at the exit of the circuit in all cases. This observation was consistent between all 11 VTs, all with a figure-eight reentry configuration.

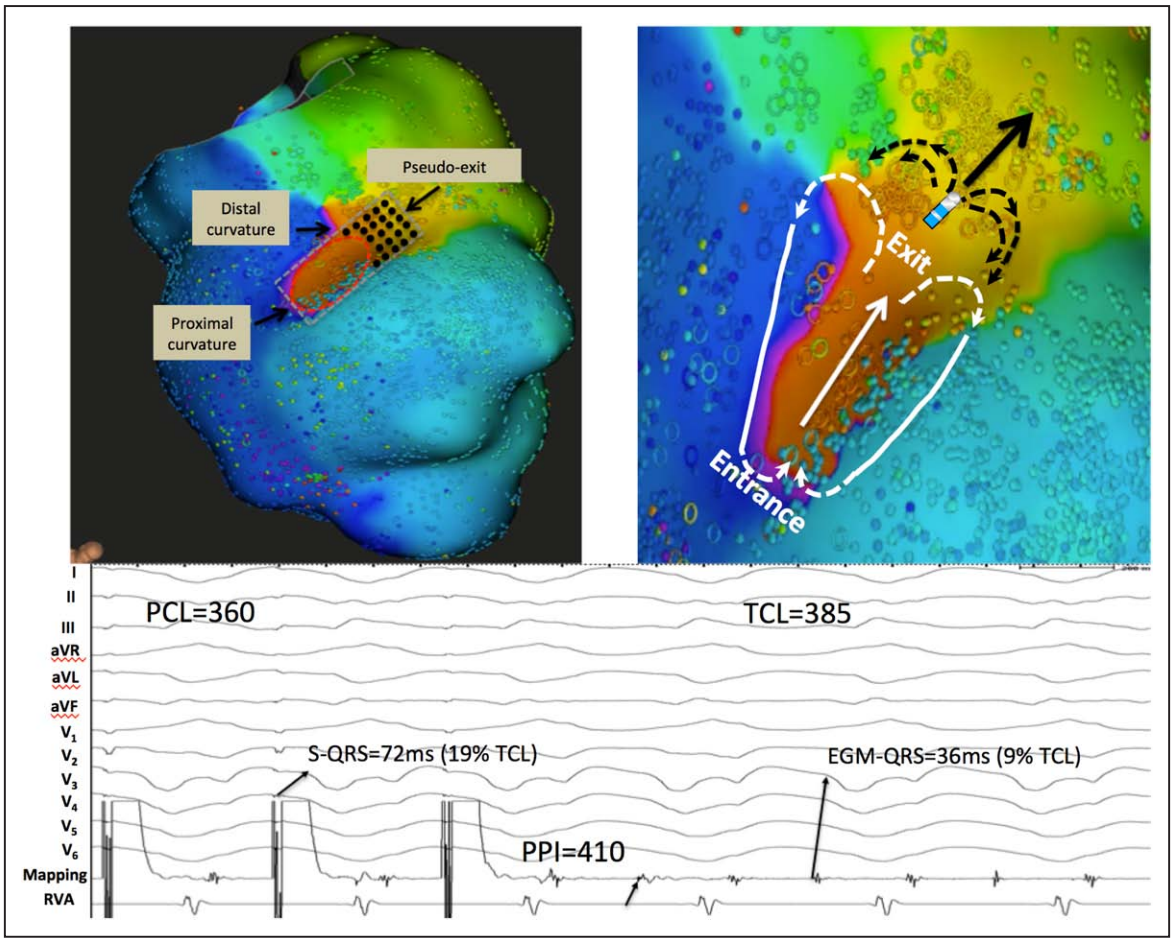

Figure 6. Entrainment criteria overestimate the dimensions of the isthmus.
Left upper, Example of a monomorphic VT mapped using both activation and entrainment techniques. The length of the isthmus determined by activation mapping was measured from the proximal curvature (entrance) to the distal curvature (exit) and is highlighted in a red dashed ellipse. Dimensions of the isthmus were also measured using standard entrainment criteria and included sites with concealed QRS on all 12 ECG leads and PPI-TCL ≤30 ms (gray dashed rectangle). Although the 2 methods similarly identified the proximal curvature (entrance) and the width of the common channel, entrainment mapping overestimated the length of the isthmus, particularly at the exit site. The pseudoexit is the zone considered part of the circuit using entrainment mapping but not part of the circuit by activation mapping (black dots). **Lower**, An example of entrainment from a pseudoexit site (electrode, **Right upper**). The bipolar electrogram at the pacing site occurs just before the QRS complex (EGM to QRS of 36 ms; 9% of the TCL). Entrainment from this site resulted in concealed QRS fusion, as the stimulated pacing site assumes a similar wave front vector to the VT (solid arrow). However, in contrast to a true exit site, pacing from a pseudoexit site resulted in a longer PPI with PPI-TCL of 25 ms. This is because the pacing site is beyond the distal curvature (white arrows) and propagation of its wave front in the figure-8 configuration (black arrows) assume a curvature shape that encounters a partially refractory tissue, both result in slower conduction and prolonged postpacing interval. EGM indicates electrogram; PPI, postpacing interval; and TCL, tachycardia cycle length.

Table. Response to Overdrive Pacing at Various Zones of the Reentrant Circuit

Site	EGM	QRS Morphology	PPI-TCL, ms	EGM-QRS, % of TCL
Proximal curvature (entrance)	Fractionated (85%)	Concealed (5/7)	16±12	50–85
	Split (24%)	Fused (2/7)		
Common channel (midisthmus)	Split (90%)	Concealed (7/7)	5±2	25–50
	Fractionated (41%)			
Distal curvature (exit)	Fractionated (87%)	Concealed (17/17)	5±5	10–25
	Split (39%)			
Pseudoexit *	Fractionated (82%)	Concealed (6/6)	22±8	0–10
	Split (27%)			
Outer loop	Split (78%)	Fused (11/11)	9±6	Negative (within the QRS)
	Fractionated (44%)			

EGM indicates electrogram; PPI, postpacing interval; and TCL, tachycardia cycle length.

To preserve the ventricular structure for future correlation with the underlying substrate, we did not perform ablation at critical sites that could have potentially altered the tissue and limit histological analysis. However, the accuracy of the activation mapping was additionally validated by the response to subthreshold stimulation from different zones of the circuit. Although we did not systematically perform subthreshold stimulation testing as part of the protocol, overdrive pacing at an output that was too low to capture the ventricular tissue occurred in 9 midisthmus sites and in 14 nonisthmus sites. Subthreshold pacing from isthmus sites terminated the VT in 5 of the 9 cases (3 separate circuits in 3 different animals). In particular, in 1 of these 3 circuits, subthreshold stimulation from the isthmus terminated the VT reproducibly 3 repeated times (Figure 7). In contrast, subthreshold stimulation from nonisthmus sites did not terminate the VT (0/14 in 4 different animals).

DISCUSSION

Major Findings

1. This study demonstrates the feasibility to map reentrant VTs using Rhythmia high-resolution mapping technology. It allows detailed activation mapping of the reentrant circuit, including its protected isthmus.
2. The zone(s) of slow conduction within the reentrant circuit are the inward (entrance) and outward (exit) curvatures, whereas conduction velocity in the common channel itself is nearly normal.
3. The common channel is protected by laterally opposing lines of functional block. These allow a very slow transverse conduction that is sufficiently slow to protect the common channel, allowing parallel propagation of the orthodromic wave front.
4. Conduction velocities within the reentrant circuit are dynamic and influenced by the vector of wave front propagation, such that the zone of slow conduction is not geometrically fixed, but rather influenced by properties of anisotropic conduction.
5. Entrainment mapping overestimates dimensions of the isthmus. Specifically, exit sites based on entrainment criteria may be well past the true exit as determined by activation.

In this study, we used a novel multielectrode mapping catheter capable of acquiring up to 64 simultaneous electrograms at each tachycardia beat, thus facilitating data acquisition and reducing mapping time. The increased number of electrograms combined with the small and closely spaced electrodes allowed in vivo mapping of infarct-related reentrant VT with a median spatiotemporal resolution of 52 electrograms/cm.[2] Activation maps were constructed at 10-ms isochrone steps.

Activation maps of postinfarction reentrant VTs demonstrated distinct electrophysiological elements of reentry, including: (1) entrance of the orthodromic wave front into a protected channel; (2) protected channel isthmus bounded by 2 laterally opposing lines (functional) block, allowing orthogonal conduction of the orthodromic wave front in the isthmus; (3) exit of the orthodromic wave front into the remainder ventricle; (4) outer loops(s) consisting of wave front propagating along the outer margin of the isthmus; and (5) remote ventricular sites that are not part of the reentrant circuit.

Geometric Architecture of the Circuit

In this model of chronic anterior wall infarction, the predominant circuit configuration was a double loop (figure-of-eight) reentry as originally described by El Sherif.[14] The axis of the isthmus was uniformly paral-

Figure 7. Subthreshold stimulation from a midisthmus site with VT termination.
This is an example of a sustained monomorphic ventricular tachycardia (VT) with a cycle length of 280 ms. Pacing from a midisthmus site at a cycle length of 240 ms captured the local tissue (small dashed arrows), however failed to capture the tachycardia. The fourth pacing stimulus terminates the tachycardia without capture of the ventricle (red star). The fifth and seventh pacing stimuli capture the ventricle with QRS morphology similar to the tachycardia and a long stimulus to QRS interval. These findings are consistent with subthreshold stimulation with VT termination at or near an isthmus site.

lel to the long axis of the ventricle and bounded by 2 parallel lines of block. This observation is consistent with postinfarction VT in the canine model. Wit and colleagues[6] mapped the epicardium of subacute canine left anterior descending infarcts using an array of 192 bipolar electrodes during sustained VT. They found that lines of block during tachycardia were similarly oriented parallel to the long axis of the LV, from base to apex. This appears to be consistent also in our human data of patients with left anterior descending infarction mapped with high-resolution mapping technologies (unpublished data). However, this may not be the case for all infarct-related VT. In particular, in patients with chronic infarction and ventricular aneurysm, the most obvious pathway for circulating excitation would be the rim of the surviving myocardium around the scar or an anatomic barrier (ie, mitral annulus).[15,16]

Dimension of the Isthmus

We measured the dimensions of the isthmus in 18 tachycardias with detailed activation maps. Dimensions of the isthmus were relatively consistent, measuring ≈15 mm in length and 7 mm in width. These findings are consistent with isthmus dimensions in humans. de Bakker and colleagues performed detailed mapping of 139 VTs in patients with healed myocardial infarction in the operating room. The average isthmus size was 1.4 cm^2.[17] In comparison, de Chillou and colleagues[18] reported significantly larger isthmus dimensions of 31±7 mm long by 16±8 mm wide. This discrepancy may be attributable to the differences in measurement techniques and mapping resolution. These authors measured the width of isthmus as the conductive myocardial tissue delineated by 2 parallel lines of nonconductive tissue (sites with electrograms demonstrating double potentials). Although this concept is valid, double potentials can be recorded over a broad area and may thus overestimate the width of the isthmus. In addition, the authors did not report the method used to measure the length of the isthmus and may have well overestimated its size. We believe that the most significant differences in measurements stem from the difference in mapping resolution: lower mapping resolution techniques may overestimate (and also underestimate) the size of the isthmus because of the interpolation of activation times in undersampled areas.

Lines of Block or Pseudoblock

In general, reentrant circuits occur around a region of conduction block. This is crucial for reentry because it prevents the reentrant impulse from short circuiting the reentrant pathway.[6] The region of block around which excitation revolves may result either from an anatomic obstacle (eg, scar tissue or valvular annuli) or may be caused by functional properties of viable cardiac fibers as in the leading circle mechanism.[19] We found that these lines of block did not truly block conduction, but allowed slow transverse conduction through them: in the presence of true block, activation waves on either side of the line should move toward each other or perpendicular to one another; however, we found that activation waves moved toward the same direction, suggesting a slow conduction through the line (Figure 4). In support of this, many of the electrograms at the lines of block had long- and low-amplitude fractionated activity between the split potentials, consistent with lack of true block (Figure 1). This observation is consistent with computer modeling of postinfarction reentrant VT circuits and with experiments in the dog model of infarction with VT.[6,20] Distinction between true lines of block (as are often present during initiation of the tachycardia by premature impulses) and lines of functional block highlights the importance of mapping resolution (special resolution as a function of the number of electrodes per unit area) and potential errors because of the interpolation of activation times. The distinction between line of true conduction block and line of functional block during tachycardia may not be important in terms of practice. However, it may have significant implications for mapping the VT substrate during sinus where block may or may not be present, depending on the pacing rate, coupling interval of the premature impulse, and the vector of wave front propagation.

Conduction Velocities in the Circuit

We found that conduction velocities were slowest at entrance and exit sites, but rather normal at the common channel (isthmus) of an anterior myocardial infarction. These observations are consistent with computer modeling and experiments in postinfarction canine.[1] Ciaccio and colleagues[1] showed that the curvature at entry points is often the slowest conducting area and associated with marked nonuniform anisotropic conduction as evident by fractionated electrograms. Biophysically, an extracellular waveform with >1 deflection can be accounted for only by asynchronous firing of ≥2 groups of cells that are separated by areas in which there is diminished or absent cell-to-cell electric coupling in the path of propagation.[21] In postinfarction hearts, this is usually attributable to fibrosis, forming isolating barriers and discontinuities resulting in nonuniform anisotropic properties and zigzag course of activation.[2] Additional factors that contribute to nonuniform anisotropic conduction include abrupt change in the vector of activation, increased axial resistivity, and thickness gradient often present at the infarct border zone.[1,22] In particular, conduction that is parallel to the fiber orientation is relatively rapid, whereas conduction that is perpendicular to the fiber direction is about 10 times slower. This may explain the relatively rapid conduction velocity in the common channel because the orthodromic wave front propagates in parallel to the fiber direction. In contrast, entrance and exit sites are highly curved and hence slower. Entrance sites are particularly slow because of the convergence of 2 opposing wave fronts of activation as in double-loop reentrant circuits.

Limitations of Entrainment

We found that standard entrainment criteria overestimate the true size of the isthmus, particularly at its exit site, such that concealed QRS fusion combined with PPI-TCL ≤30 ms can occur beyond the distal curvature. We termed these sites pseudoexit sites to distinguish them from true exit sites at the distal curvature. Pacing at pseudoexit sites resulted in concealed QRS fusion likely because of a similar orthodromic activation wave front with concealed antidromic fusion. This may be particularly true in double-loop reentry because pacing just distal to an exit site results in a point source activation pattern with propagation in multiple directions (Figure 7). However, in contrast to true exit sites, pacing from pseudoexit sites resulted in a longer PPI (Table). We speculate that this may be attributable to increased curvature gradient (resistance) and activation of partially depolarized tissue resulting in a slower conduction velocity. However, this requires additional investigation with resetting curves at different zones of the circuits. From a clinical standpoint, this may explain why ablation at exit sites determined by entrainment can fail to terminate the VT and often results in change of the tachycardia or the inducibility of multiple similar morphologies with minor variations in the exit site.[23]

Study Limitations

This study was performed in swine and used an established humanlike model of subendocardial infarction and VT. However, it requires validation in humans, and particularly in patients with nonanterior wall infarction, patients with unstable VT, and patients with noncoronary scar-related VT. In these patients, the substrate may be different in terms of the extent of conduction abnormalities, area and depth of scar, commonly producing cardiac arrest as opposed to stable monomorphic VT. Our initial clinical experience in humans with coronary disease and VT has thus far been consistent with these findings, particularly in patients with chronic anterior wall infarction. Conduction velocities were calculated using the single-vector method with the assumption that the tissue is homogeneously anisotropic and 2-dimensional (we did not

measure full-thickness activation times). Although this may skew the velocity measurements, because the VT substrate in this model is subendocardial, 2-dimensional endocardial data may still allow good representation of the overall conduction velocities within the tissue. In addition, because conduction velocities were measured from 2-dimensional data, it assumes that electric conduction wave front takes the shortest route. As such, the relatively normal conduction velocity at the isthmus may potentially reflect slower conduction of a longer zigzag course. Accurate velocity measurements will require mapping with full-thickness plunge electrodes. Although pacing sites were determined and marked using the electroanatomical mapping system, pacing may have resulted in capture of locally adjacent tissue. Although this may be a limitation of comparing activation mapping and response to pacing, the differences were consistent and restricted to pseudoexit sites only. In this regard, the findings of this study relied on the use of a novel high-resolution mapping technology and require further validation with other mapping technologies as they increasingly become available. Last, the correlation between the VT circuit and the underlying substrate, in particular, the relationship between conduction velocities and presence of block (or pseudoblock) during sinus/pacing and VT were not included in this report because of space limitation, and will be described in separate article.

SOURCES OF FUNDING

This study was supported in part by Boston Scientific and National Institutes of Health grant 1R21HL127650-01 and 1R01HL129185.

DISCLOSURES

Dr Anter receives research grants from Biosense Webster, research grants and speaking honoraria from Boston Scientific. Dr Josephson receives research grants and speaking honoraria from Medtronic. Dr Buxton receives research grants from Biosense-Webster and Medtronic, Inc. C. Tschabrunn receives research grants from Biosense Webster.

AFFILIATIONS

From Harvard-Thorndike Electrophysiology Institute, Cardiovascular Division, Department of Medicine, Beth Israel Deaconess Medical Center, Harvard Medical School, Boston, MA.

FOOTNOTES

Received February 8, 2016; accepted May 5, 2016.

The online-only Data Supplement is available with this article at http://circ.ahajournals.org/lookup/suppl/doi:10.1161/CIRCULATIONAHA.116.021955/-/DC1.

Circulation is available at http://circ.ahajournals.org.

REFERENCES

1. Ciaccio EJ, Ashikaga H, Kaba RA, Cervantes D, Hopenfeld B, Wit AL, Peters NS, McVeigh ER, Garan H, Coromilas J. Model of reentrant ventricular tachycardia based on infarct border zone geometry predicts reentrant circuit features as determined by activation mapping. *Heart Rhythm*. 2007;4:1034–1045. doi: 10.1016/j.hrthm.2007.04.015.
2. de Bakker JM, van Capelle FJ, Janse MJ, Tasseron S, Vermeulen JT, de Jonge N, Lahpor JR. Slow conduction in the infarcted human heart. 'Zigzag' course of activation. *Circulation*. 1993;88:915–926.
3. Peters NS, Wit AL. Myocardial architecture and ventricular arrhythmogenesis. *Circulation*. 1998;97:1746–1754.
4. Wit AL, Peters NS. The role of gap junctions in the arrhythmias of ischemia and infarction. *Heart Rhythm*. 2012;9:308–311. doi: 10.1016/j.hrthm.2011.09.056.
5. Fenoglio JJ Jr, Pham TD, Harken AH, Horowitz LN, Josephson ME, Wit AL. Recurrent sustained ventricular tachycardia: structure and ultrastructure of subendocardial regions in which tachycardia originates. *Circulation*. 1983;68:518–533.
6. Dillon SM, Allessie MA, Ursell PC, Wit AL. Influences of anisotropic tissue structure on reentrant circuits in the epicardial border zone of subacute canine infarcts. *Circ Res*. 1988;63:182–206.
7. Reddy VY, Reynolds MR, Neuzil P, Richardson AW, Taborsky M, Jongnarangsin K, Kralovec S, Sediva L, Ruskin JN, Josephson ME. Prophylactic catheter ablation for the prevention of defibrillator therapy. *N Engl J Med*. 2007;357:2657–2665. doi: 10.1056/NEJMoa065457.
8. Ciaccio EJ, Tosti AC, Scheinman MM. Relationship between sinus rhythm activation and the reentrant ventricular tachycardia isthmus. *Circulation*. 2001;104:613–619.
9. Tschabrunn CM, Roujol S, Nezafat R, Faulkner-Jones B, Buxton AE, Josephson ME, Anter E. A swine model of infarct-related reentrant ventricular tachycardia: Electroanatomic, magnetic resonance, and histopathological characterization. *Heart Rhythm*. 2016;13:262–273. doi: 10.1016/j.hrthm.2015.07.030.
10. Anter E, Tschabrunn CM, Contreras-Valdes FM, Li J, Josephson ME. Pulmonary vein isolation using the Rhythmia mapping system: Verification of intracardiac signals using the Orion mini-basket catheter. *Heart Rhythm*. 2015;12:1927–1934. doi: 10.1016/j.hrthm.2015.05.019.
11. Stevenson WG, Khan H, Sager P, Saxon LA, Middlekauff HR, Natterson PD, Wiener I. Identification of reentry circuit sites during catheter mapping and radiofrequency ablation of ventricular tachycardia late after myocardial infarction. *Circulation*. 1993;88(4 pt 1):1647–1670.
12. Linnenbank AC, de Bakker JM, Coronel R. How to measure propagation velocity in cardiac tissue: a simulation study. *Front Physiol*. 2014;5:267. doi: 10.3389/fphys.2014.00267.
13. Kléber AG, Janse MJ, Wilms-Schopmann FJ, Wilde AA, Coronel R. Changes in conduction velocity during acute ischemia in ventricular myocardium of the isolated porcine heart. *Circulation*. 1986;73:189–198.
14. el-Sherif N, Gough WB, Zeiler RH, Hariman R. Reentrant ventricular arrhythmias in the late myocardial infarction period. 12. Spontaneous versus induced reentry and intramural versus epicardial circuits. *J Am Coll Cardiol*. 1985;6:124–132.
15. Frame LH, Page RL, Hoffman BF. Atrial reentry around an anatomic barrier with a partially refractory excitable gap. A canine model of atrial flutter. *Circ Res*. 1986;58:495–511.
16. Anter E, Li J, Tschabrunn CM, Nezafat R, Josephson ME. Mapping of a post-infarction left ventricular aneurysm-dependent macroreentrant ventricular tachycardia. *HeartRhythm Case Rep*. 2015;1:472–476. doi: 10.1016/j.hrcr.2015.07.011.
17. de Bakker JM, van Capelle FJ, Janse MJ, Wilde AA, Coronel R, Becker AE, Dingemans KP, van Hemel NM, Hauer RN. Reentry as

a cause of ventricular tachycardia in patients with chronic ischemic heart disease: electrophysiologic and anatomic correlation. *Circulation*. 1988;77:589–606.
18. de Chillou C, Lacroix D, Klug D, Magnin-Poull I, Marquié C, Messier M, Andronache M, Kouakam C, Sadoul N, Chen J, Aliot E, Kacet S. Isthmus characteristics of reentrant ventricular tachycardia after myocardial infarction. *Circulation*. 2002;105:726–731.
19. Allessie MA, Bonke FI, Schopman FJ. Circus movement in rabbit atrial muscle as a mechanism of tachycardia. III. The "leading circle" concept: a new model of circus movement in cardiac tissue without the involvement of an anatomical obstacle. *Circ Res*. 1977;41:9–18.
20. Maglaveras N, De Bakker JM, Van Capelle FJ, Pappas C, Janse MJ. Activation delay in healed myocardial infarction: a comparison between model and experiment. *Am J Physiol*. 1995;269(4 pt 2):H1441–H1449.
21. Spach MS. Anisotropy of cardiac tissue: a major determinant of conduction? *J Cardiovasc Electrophysiol*. 1999;10:887–890.
22. Rohr S, Kucera JP, Fast VG, Kléber AG. Paradoxical improvement of impulse conduction in cardiac tissue by partial cellular uncoupling. *Science*. 1997;275:841–844.
23. Costeas C, Peters NS, Waldecker B, Ciaccio EJ, Wit AL, Coromilas J. Mechanisms causing sustained ventricular tachycardia with multiple QRS morphologies: results of mapping studies in the infarcted canine heart. *Circulation*. 1997;96:3721–3731.